

Nanoscale

Accepted Manuscript

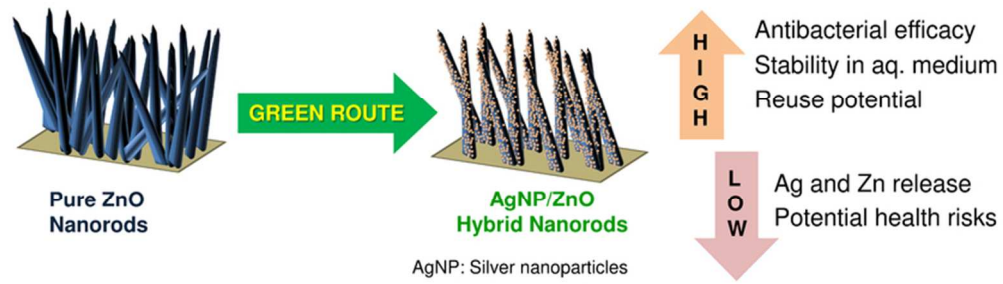


This is an *Accepted Manuscript*, which has been through the Royal Society of Chemistry peer review process and has been accepted for publication.

Accepted Manuscripts are published online shortly after acceptance, before technical editing, formatting and proof reading. Using this free service, authors can make their results available to the community, in citable form, before we publish the edited article. We will replace this *Accepted Manuscript* with the edited and formatted *Advance Article* as soon as it is available.

You can find more information about *Accepted Manuscripts* in the [Information for Authors](#).

Please note that technical editing may introduce minor changes to the text and/or graphics, which may alter content. The journal's standard [Terms & Conditions](#) and the [Ethical guidelines](#) still apply. In no event shall the Royal Society of Chemistry be held responsible for any errors or omissions in this *Accepted Manuscript* or any consequences arising from the use of any information it contains.



A dual mode of antibacterial action of Ag/ZnO nanomaterial was envisaged, which retain antibacterial efficacy even after multiple reuse without inducing human cytotoxicity
70x21mm (300 x 300 DPI)

Cite this: DOI: 10.1039/c0xx00000x

www.rsc.org/xxxxxx

FULL PAPER

Arginine assisted immobilization of silver nanoparticles on ZnO nanorods: An enhanced and reusable antibacterial substrate without human cell cytotoxicity

Shekhar Agnihotri,^a Geetika Bajaj,^a Suparna Mukherji,^{a,b} and Soumyo Mukherji^{a,c,d*}

⁵ Received (in XXX, XXX) Xth XXXXXXXXX 20XX, Accepted Xth XXXXXXXXX 20XX

DOI: 10.1039/b000000x

Silver-based hybrid nanomaterials are gaining interest as potential alternatives for conventional antimicrobial agents. Herein, we present a simple, facile and eco-friendly approach for deposition of silver nanoparticles (AgNPs) on ZnO nanorods, which behave as a nanoreactor for *in-situ* synthesis and also as an immobilizing template in the presence of arginine. The presence of arginine enhanced the stability of ZnO deposition on the glass substrate by hindering the dissolution of zinc under alkaline conditions. Various Ag/ZnO hybrid nanorod (HNR) samples were screened so as to obtain high amount of silver immobilization on the ZnO substrate. Ag/ZnO HNRs displayed potent antibacterial ability and could achieve 100% kill for both, *Escherichia coli* and *Bacillus subtilis* strains under various test conditions. The hybrid material mediated its dual mode of antibacterial action through direct contact-kill and release of silver ions/nanoparticles and showed superior bactericidal performance compared to pure ZnO nanorods and colloidal AgNPs. No significant decline in antibacterial efficacy was observed even after the same substrate was repeatedly reused multiple times. Interestingly, the amount of Ag and Zn release was much below their maximal limit in drinking water thus, preventing potential health hazards. Immobilized AgNPs showed no cytotoxic effects on human hepatocarcinoma cell line (HepG2). Moreover, exposing cells with the antibacterial substrate for 24 hours did not lead to significant generation of reactive oxygen species (ROS). The good biocompatibility and bactericidal efficacy would thus make it feasible to utilize this immobilization strategy for preparing new generation antibacterial coatings.

1. Introduction

Considering the potential health risks associated with the emergence of multidrug-resistant bacteria and greater incidences of cross contamination, development of new and effective bactericidal agents is of utmost concern.^{1, 2} The interest in nano-silver based antimicrobial materials is increasing worldwide and is corroborated by the large number of research articles published in this area during the past decade.^{3, 4} Compared to colloidal AgNPs, immobilized silver nanoparticles are physico-chemically more stable as they are less prone to aggregation and oxidation when exposed to the aqueous media.⁵⁻⁷ Thus they retain long-term antibacterial efficacy. Moreover, immobilization of silver nanoparticles on a support matrix facilitates ease in handling, reusability, and minimizes toxic effects associated with their inevitable discharge into the aqueous ecosystem.^{7, 8} Reportedly, silver nanoparticles can be incorporated on hybrid materials either by impregnating AgNPs within porous matrices⁹ or by anchoring them on surface-functionalized solid supports.^{10, 11} Silver nanoparticles immobilized on various inorganic and organic substrates such as, SiO₂, Fe₂O₃, zinc oxide, and graphene

⁴⁵ have demonstrated enhanced antibacterial performance over long term use.^{7, 12-14}

Other than metallic silver, zinc oxide (ZnO) has been widely reported to inhibit and inactivate microbial growth at nanoscale. Being relatively cheaper, non-toxic, and biocompatible, ZnO is an important ingredient for various cosmetic products, antibacterial lotions, and is commonly used as a drug carrier and filler in dental materials.^{15, 16} The utilization of Ag/ZnO based hybrid nanostructures has recently gained much interest not only because of their ease of fabrication through various routes, but also due to their comparatively higher photocatalytic efficiency and synergistic antibacterial activity than their individual forms.^{16, 17} Till date, a variety of methods have been explored for incorporation of Ag on to ZnO support material through doping, ultrasonication, solvothermal method, pulsed layer deposition, irradiation assisted anchoring or *in-situ* synthesis of AgNP.^{13, 18-21} From the point of view of immobilization, silver nanoparticles can readily self-assemble on ZnO templates as they provide both anchoring sites for the metal ions to bind and also nucleation sites for their subsequent growth. However, in the absence of any binder/linker, it is extremely difficult to control the dispersivity,

stability and loading of silver nanoparticles over ZnO surfaces.²⁰ As a result, AgNPs may get easily desorbed from ZnO surface when exposed to harsh experimental conditions thereby limiting its long term usage. Therefore, it is highly desirable to develop an effective approach for localized deposition of AgNPs on the surface-functionalized ZnO nanostructures without compromising their bactericidal efficacy.

Amino acids possess high affinity towards metals and metal oxides. Among all the amino acids, arginine has the highest affinity towards silver ions,²² which may bind at various electron rich sites, *i.e.*, nitrogen atoms of α -amino group as well as guanidino side chain, in addition to carboxyl moieties at C-terminus, forming stable silver-arginine complexes. On the other hand, arginine is also known to involve in surface modification of zinc oxide as ZnO-binding polypeptide.^{23, 24} However, to the best of our knowledge, arginine assisted immobilization of silver nanoparticles on ZnO nanorods under ambient conditions has not been attempted till date.

Although considerable success has been achieved for enhancing the bactericidal action of Ag/ZnO nanocomposites, surprisingly, some important aspects are yet to be explored. There are only limited number of reports in which Ag/ZnO nanocomposites have been evaluated on the basis of their silver/zinc release in aqueous media, reusability, durability, long-term antimicrobial efficacy and cytotoxic effects on human or mammalian cells. Li *et al.*¹³ recently demonstrated the long-term antimicrobial activity and reusability of Ag/ZnO nanomaterial for wound dressing applications. Similarly, Motshekgwa *et al.*²⁰ have reported better disinfection performance of Ag/ZnO nanocomposite supported on Bentonite clay, where the leaching of silver from the nanocomposite was found to be within the acceptable limits specified for potable water. However, in order to establish the biocidal potential of Ag/ZnO hybrid nanomaterial for diverse applications, all the aforementioned aspects needs to be discussed in one study.

In this study, we describe a facile and greener approach for dense immobilization of silver nanoparticles on ZnO nanorods using arginine as the linker molecule for potential antibacterial purposes. The reaction conditions were optimized to achieve maximum immobilization of AgNPs over ZnO nanorods so as to maximize the bactericidal potential. Antibacterial tests for Ag/ZnO hybrid material against both Gram-positive and Gram-negative bacterial strains were performed at two initial cell concentrations (10^3 CFU ml⁻¹ and 10^5 CFU ml⁻¹) in a 100 ml batch reactor. The bactericidal efficacy and corresponding silver release profile of the same AgNP/ZnO substrate was also evaluated over multiple wash and reuse cycles in order to determine its potential for practical applications. Cytotoxicity analysis of hybrid biomaterial was determined against human HepG2 cell line as an *in-vitro* model to test its biocompatibility and applicability as antibacterial coatings for promising biomedical applications.

2. Experimental Details

Materials required

Zinc acetate dihydrate ($\text{Zn}(\text{CH}_3\text{COO})_2 \cdot 2\text{H}_2\text{O}$, $\geq 98\%$ pure), Zinc nitrate hexahydrate ($\text{Zn}(\text{NO}_3)_2 \cdot 6\text{H}_2\text{O}$, $\geq 98\%$ pure), and Lithium

hydroxide monohydrate ($\text{LiOH} \cdot \text{H}_2\text{O}$, $\geq 98\%$ pure) were received from Sigma-Aldrich (USA). Hexamethylenetetramine (HMTA, $\text{C}_6\text{H}_{12}\text{N}_4$, $\geq 99\%$ pure), silver nitrate (AgNO_3 , $>99.9\%$ pure), L-arginine ($\text{C}_6\text{H}_{14}\text{N}_4\text{O}_2$, $\geq 99\%$ pure) and ascorbic acid ($\text{C}_6\text{H}_8\text{O}_6$, $\geq 99\%$ pure) were purchased from Merck (India). *Escherichia coli* MTCC 443 (ATCC 25922) and *Bacillus subtilis* MTCC 441 (ATCC 6633) were used as test strains for conducting antibacterial experiments. They were originally procured from the Institute of Microbial Technology (Chandigarh, India). Nutrient media (Himedia Pvt. Ltd., Mumbai) was used for growing bacteria in liquid broth culture as well as preparing solid media for plate culture studies by adding 2% bacteriological agar (Himedia Lab. Ltd., Mumbai).

For cytotoxicity tests, human hepatocarcinoma cell lines (HepG2) were obtained from the National Centre for Cell Sciences, Pune, India. Phosphate buffered saline (PBS) was purchased from Himedia Pvt. Ltd., Mumbai, India. Dulbecco's modified Eagle's medium (DMEM), fetal bovine serum, 10^4 U ml⁻¹ penicillin, 10 mg ml⁻¹ streptomycin, and 25 μg ml⁻¹ Amphotericin-B were procured from Gibco (USA). (3-(4, 5-dimethyl- thiazol-2-yl)-2, 5-diphenyl tetrazolium bromide (MTT) dye, Triton X-100, tertiary butyl hydroperoxide (t-BH) and 2,7-dichlorofluorescein diacetate (DCFDA) dye were purchased from Sigma-Aldrich (USA). All chemicals were used as received without further purification. Ultrapure water (resistivity 18.2 M Ω cm) was used for all synthesis reactions and bacteriological experiments.

Synthesis of AgNP-ZnO hybrid nanorods

ZnO nanorods were synthesized through a two-step alcohothermal seeding and hydrothermal growth process (refer to Section S1† in ESI). Aqueous solution of arginine-silver complexes was prepared as reported earlier.²⁵ Five sets of silver-arginine complexes (aq.) were synthesized having the molar concentrations of AgNO_3 as 5, 10, 20, 25, and 75 mM such that the molar ratio of silver : arginine was kept constant at 5:2. ZnO NRs grown on glass surfaces ($2 \times 2.3 \text{ cm}^2$) were immersed in freshly prepared silver-arginine mixture of various concentrations (5 to 75 mM) for 12 hours so as to facilitate interaction between the ZnO NRs with the silver-arginine complex. Subsequently, the substrates were removed, washed with DI water and sonicated for 10 seconds to remove loosely bound silver. This was followed by *in-situ* reduction of silver ions using a non-toxic reducing agent, *i.e.*, ascorbic acid. The silver loaded ZnO glass substrates were dipped in ascorbic acid solution (100 mM, 50 ml) for 30 minutes resulting in *in-situ* reduction followed by immobilization of AgNPs over the surface of ZnO NRs. Samples were thoroughly rinsed and sonicated as mentioned in the earlier step. To designate various AgNP-ZnO hybrid nanorod (HNR) samples, substrates incubated in silver-arginine solution mixture containing 5 mM, 10 mM, 20 mM, 25 mM, and 75 mM AgNO_3 are referred as Ag/ZnO-5, Ag/ZnO-10, Ag/ZnO-20, Ag/ZnO-25, and Ag/ZnO-75 HNRs respectively, in the following studies. The mass loading of silver in the immobilized substrates was quantified using inductively coupled plasma-atomic emission spectroscopy (ICP-AES, refer to Section S2† in ESI). Finally, the silver content on Ag/ZnO HNRs ($\mu\text{g cm}^{-2}$) was calculated by normalizing the amount of silver extracted from the substrate, with the total surface area of Ag/ZnO HNRs deposited on the

glass substrate.

Antibacterial studies

Strain specific antibacterial activity of Ag-ZnO HNRs was determined against Gram-negative *Escherichia coli* MTCC 443 and Gram-positive *Bacillus subtilis* MTCC 441 strains. Two set of independent antibacterial tests were performed using deionized water (DI) and a chlorine-free phosphate buffer as the test solution, as described in our earlier study.⁷ Ag-ZnO glass substrate (2 x 2.3 cm²) was suspended centrally in a batch reactor (100 ml) having either 10³ or 10⁵ CFU ml⁻¹ initial bacterial concentration and sampling was performed over a period of 1-2 hours. Size-controlled, monodispersed colloidal AgNPs of average size 10 ± 2 nm, synthesized following the protocol discussed in our recent study²⁶ were used in antibacterial studies for comparing their bactericidal activity with immobilized Ag/ZnO HNRs. The total mass of silver in colloidal AgNPs (in the 100 ml batch reactor) was kept as 6.0 x 10⁻² mg, which was similar to that in the immobilized system (*i.e.*, Ag/ZnO HNRs). Silver nanoparticles immobilized on a flat amine functionalized silica substrate⁷ (AgNP-silica) was also considered in order to compare the two 'immobilized systems' *i.e.*, AgNP-silica and Ag/ZnO HNRs for their antibacterial action under similar test conditions. For each experiment, the bacterial aliquots (100 µl) were homogenously plated on agar plates, and incubated at 37°C to count the viable bacterial colonies after 24 hours. All studies were done in duplicate. Zone of inhibition (ZoI) assay was done to compare the bactericidal potential of AgNP/ZnO HNR substrates with that of pure ZnO NRs. For this, the substrates were individually placed on an agar plate having uniform bacterial suspension (*E. coli* MTCC 443, 10⁵ to 10⁶ CFU ml⁻¹) and the culture plates were incubated at 37°C for 24 hours. Both substrates (*i.e.*, AgNP/ZnO HNRs and Pure ZnO NRs) were screened on the basis of the zone of inhibition (ZoI) using photographic images of the culture plates. For determining the contact-killing biocidal action of the material, Ag/ZnO-20 HNRs deposited on glass substrate (2 x 2.3 cm²) was placed in direct contact with solid agar having uniform bacterial lawn (*E. coli*, 10⁵-10⁶ CFU ml⁻¹) for one hour to express its antibacterial effects. After one hour, the substrate was carefully removed and the culture plate was incubated for 24 hours at 37°C.

To demonstrate the reuse potential of the hybrid antibacterial material, a single AgNP-ZnO HNR substrate was utilized several times for disinfection experiments. Concurrently, the silver and/or zinc release profile was also evaluated. The same antibacterial substrate (2 x 2.3 cm²) was used 11 times alternately, such that each *n*th and *n*+1th study denotes a disinfection study and a silver/zinc release study, respectively (where, *n*= 1, 3, 5, 7...). After each study, the substrate was immediately removed from the test solution, washed with DI water, dried with nitrogen gas purging and stored in a vacuum desiccator until the next use. Silver release studies were performed under similar reaction conditions in DI water devoid of any bacterial cells. Predetermined volume of samples was taken at regular intervals followed by acid digestion using dil. HNO₃ (0.1 M). After acid digestion, the samples were analyzed for silver and zinc released using ICP-AES. Standard solutions were used for the calibration. The time lag between disinfection and silver release studies was maintained as 10-12 hours in order

to minimize the variability.

Mechanism of antibacterial action

To demonstrate the mechanism of the biocidal action of Ag/ZnO HNRs, *E. coli* cells (each at 10⁶-10⁷ CFU ml⁻¹) were treated with Ag/ZnO-20 substrate (2 x 2.3 cm²) for 6 hours. Untreated *E. coli* cells were used as control. The treated cells were harvested by centrifugation (5000 rpm, 10 min.) and washed thrice with DI water to remove the loosely bound Ag or Zn over the bacterial surface. A series of pre-treatment steps were followed for electron microscopy analysis. Primary fixation of bacterial cells was achieved using 2.5% glutaraldehyde for 1 hour. After intermediate washing steps, secondary fixation was performed using 1% OsO₄ in dark for 30 minutes. Phosphate buffer medium (pH 7.2) was used for washing the bacterial cells before and after the fixation steps. The samples were subsequently dehydrated with a graded ethanol series (30%, 50%, 70%, 90%, 95%, 100%) followed by staining with 3% uranyl acetate. Bacterial cells were drop casted on carbon coated Cu grids and were air dried at room temperature for field emission gun-transmission electron microscope (FEG-TEM) analysis. For field emission gun-scanning electron microscope (FEG-SEM) analysis, bacterial cells loaded on Cu grids were examined without any conductive coating (gold/platinum/gold-palladium sputtering) to reduce possible artifact.

In-vitro cytotoxicity and intracellular ROS generation

Human hepatocarcinoma cells (HepG2) were cultured in Dulbecco's modified Eagle's medium supplemented with 10% fetal bovine serum, 100 U ml⁻¹ penicillin, 100 µg ml⁻¹ streptomycin, and 25 µg L⁻¹ Amphotericin-B in a 24-well plate. Cells (1 x 10⁵ cells) were grown for 24 hours at 37°C under the humidified atmosphere containing 5% CO₂/95% air. (3-(4, 5-dimethyl- thiazol-2-yl)-2, 5-diphenyl tetrazolium bromide (MTT) assay was followed as reported earlier²⁷ with minor modifications. Before seeding the cells, Ag/ZnO-25 HNRs substrate and pristine glass slide (without any Ag/ZnO deposition) of equal dimension (1 x 1 cm²) were sterilized by dipping in 70% ethanolic solution for 2 hours followed by UV radiation for 30 minutes. A single Ag/ZnO HNR substrate (1 x 1 cm²) was placed at the bottom of each well in the 24-well plate. HepG2 cells (200µl in each well) were treated with Ag/ZnO HNRs for different time periods (6, 12, 24 and 48 hours) as four independent studies set-up in triplicate. Control experiments were carried out using 1% Triton X-100 (positive control), which causes 100% toxicity to cells. Treated cells were subsequently incubated in MTT dye (1 mg ml⁻¹) for 4 hours in the dark. Cell viability was evaluated by the ability of metabolically active cells to reduce MTT into the insoluble, purple formazone crystals. After incubation for the desired time period, the medium from each well was discarded and the resulting formazon crystals were dissolved in a 200 µl solution containing 10% sodium dodecyl sulphate and 0.01 N HCl. The absorbance was measured at 570 nm in a multiwell plate-reader (Bio-Tek, Winooski, USA). The percentage of viable cells was determined by the absorbance value of wells containing treated cells with those in untreated cells (negative control).

The intracellular ROS generation was determined using 2,7-dichlorofluorescein diacetate (DCFDA), a membrane permeable

dye which undergoes hydrolysis by esterases present within the cells. The resulting deacetylated moiety is highly sensitive to react with various ROS (mainly peroxy, hydroxyl and peroxynitrite anions) produced inside the cells and forms a fluorescent product, dichlorofluorescein (DCF). The intensity of fluorescence is therefore, proportional to the amount of ROS produced by the cells. HepG cells (1×10^5 cells) were seeded in a 24-well plate (black bottom) for 24 hours. Similar to the MTT assay, grown cells were incubated with the Ag/ZnO-25 HNRs for 6, 12, 24 and 48 hours as four independent studies set-up in triplicate. After treatment for the desired time period, the cells were washed thrice with PBS and were subsequently incubated in DCFDA dye ($20 \mu\text{M}$) for 30 minutes under dark conditions. To isolate the cells from solution, the reaction mixture was centrifuged at 2500 rpm for 10 minutes and the supernatant was discarded. The cells were redispersed in PBS ($200 \mu\text{l}$) and the fluorescence intensity was measured in a multiwell plate reader at excitation and emission wavelengths of 485 and 528 nm, respectively. Intracellular ROS level was expressed by the fold change in the mean fluorescence intensity of exposed cells with respect to the untreated cells.

3. Results and Discussion

A hybrid antibacterial material was fabricated using ZnO nanorods (ZnO NRs). ZnO NRs serve as nano-reactors for *in-situ* synthesis of silver nanoparticles concurrently providing a template for their subsequent immobilization using arginine as a linker. Arginine is known to bind silver ions via chelation and complexation mechanisms. Under alkaline conditions, arginine exists as a zwitterion and can form stable bidentate and tridentate complexes with silver.²⁵ It has been reported that bidentate complexes of silver-arginine exist in two possible forms.²² First, Ag^+ coordinates with the carbonyl oxygen and with the nitrogen of the α -amino group, forming 'charge-solvated complexes'. Else, Ag^+ is attached to the two oxygen atoms of the guanidino group of L-arginine forming 'salt bridge complexes'. Moreover, the presence of four nitrogen moieties in L-arginine and the formation of stronger Ag-N bonds to its side chain facilitates in formation of a more stable silver-arginine tridentate complexes.^{22, 28}

Although amino acids are reported to reduce silver ions and form AgNPs, introduction of silver nitrate into arginine solution did not cause any color change. Thus formation of AgNPs was not observed. Thus, it is hypothesized that Ag^+ undergoes complexation with the arginine molecule under mild alkaline conditions (pH 7-8), which lowers the standard redox potential of Ag^+/Ag thus preventing the formation of AgNPs in solution.¹⁷ We also observed that the introduction of arginine enhanced the stability of ZnO deposition on glass substrate and retarded the solubilisation of zinc under alkaline conditions. ZnO NRs grown on glass substrate were treated with aqueous silver-arginine mixture of varying concentration (5 to 75 mM) followed by ascorbic acid mediated reduction. This resulted in uniform deposition of AgNPs over the surface of ZnO NRs (Fig. 1).

Characterization

Different hybrid nanostructures (Ag/ZnO HNRs) synthesized using this approach were characterized to optimize the relative

molar concentrations of AgNO_3 and arginine that would facilitate maximum immobilization of AgNPs on the ZnO surface. Preliminary results obtained through FTIR and Raman analyses (refer to section S3† and Fig. S1† in ESI) demonstrated the role of arginine as a linker molecule by shift in the absorption spectrum of a few characteristic peaks and enhancement in Raman signals. It was demonstrated that the incorporation of AgNPs did not affect the structural morphology and integrity of ZnO surface. Moreover, the enhancement in Raman intensity can be extrapolated for qualitative determination of the extent of AgNP immobilization on various Ag/ZnO HNRs, which is primarily governed by arginine. Among various silver-arginine complexes, the mixture having 20 mM AgNO_3 concentration was expected to exhibit the most efficient immobilization of AgNPs on ZnO nanorods.

Based on a few recent studies,^{29, 30} it can be inferred that a stable silver-arginine interaction is favorable for immobilizing AgNPs on ZnO template. Aliga *et al.*²⁹ studied the extent of silver-arginine interactions in a colloidal solution using surface enhanced Raman spectroscopy (SERS) and reported a pH dependent conformational change in the structure of arginine molecule. Thus, the stability of silver-arginine interactions is strongly dependent upon the solution pH. Recently, Garrido *et al.*³⁰ also studied the effect of pH on silver-arginine interactions using SERS and analyzed that the zeta potential of the complex mixture increased from -43.5 to -35.2 mV while increasing the pH from 7 to 9. The higher pH reduced the negative charge on arginine molecules so that the molecules become less hydrophilic, and thus induces a preferential and more stable silver-arginine interaction. In this study, the pH of various silver-arginine solution mixtures were in the range of 7 to 10 and the pH of Ag/ZnO-20 was 8.6. Therefore, the best stability of Ag/ZnO-20 can be attributed either to the spatial orientation of arginine molecules or charge reduction on L-arginine molecule at pH 8.6, which may have contributed towards the most efficient silver-arginine interaction.

The quantitative estimation of Zn and Ag content on various samples, as obtained through ICP-AES analyses is summarized in Table-1. For glass substrates of equal dimensions ($2 \times 2.3 \text{ cm}^2$), the average Ag loading increased up to Ag/ZnO-20 HNRs while, for Ag/ZnO-25 and Ag/ZnO-75 HNRs, the silver loading drastically reduced. Since ZnO nanorods were grown through drop coating of ZnO seeds on the glass substrate, it was difficult to control the Zn content on each sample. Therefore, the mass ratio of Ag : Zn was taken as a parameter to determine the extent of silver immobilization on various ZnO-glass substrates. Calculated values indicate that the highest Ag : Zn ratio was obtained for Ag/ZnO-20 HNRs, validating the results obtained through FTIR and Raman analyses. In case of Ag/ZnO-20 HNRs, the mass loading of silver was calculated to be $12.83 \mu\text{g cm}^{-2}$, which is ~ 3.5 fold higher than our previous study⁷ where AgNPs were immobilized on a surface functionalized silica substrate. This is an indication of highly dense immobilization of silver nanoparticles on ZnO substrates. For all samples the amount of Zn deposition on glass substrate was controlled in between $202\text{--}221 \mu\text{g cm}^{-2}$. Using nitrogen sorption measurements, the specific surface area of Ag/ZnO-20 HNRs was found to be $57.1 \text{ m}^2 \text{ g}^{-1}$. Compared to other Ag/ZnO hybrid nanorods, Ag/ZnO-20 HNRs

demonstrated the best results using this immobilization strategy and therefore, they were used for further characterization and antibacterial studies as discussed in the following sections.

The extinction spectra were compared to characterize the effect of silver loading on the plasmonic properties of ZnO nanorods (Fig. 2a). Ag/ZnO HNRs showed a typical extinction spectrum in the visible region at about 440 nm due to the surface plasmon resonance of silver, which confirms that AgNPs were successfully immobilized over the ZnO surface. The formation of Ag/ZnO hybrid nanorods also caused a red shift (352 to 360 nm) in the extinction peak of ZnO as compared to pure ZnO nanorods. This was possibly caused by the strong interfacial coupling between immobilized AgNPs and ZnO which is reported to reduce surface defects and promote charge separation.^{31, 32} Figure 2b shows X-ray diffraction (XRD) pattern of pure ZnO and AgNP-loaded ZnO HNRs. The diffraction peaks at $2\theta = 31.8^\circ$, 34.5° , 36.3° , 56.6° , 66.4° , 67.9° , and 69.0° correspond to (100), (002), (101), (110), (200), (112) and (201) plane indicating the typical hexagonal wurtzite structure of ZnO nanorods (JCPDS card no. 36-1451). In case of AgNP-loaded ZnO HNRs, the additional diffraction peaks at $2\theta = 38.2^\circ$ (111), 43.9° (200), and 77.2° (311) depicted the face centred cubic structure of AgNPs and demonstrated that all silver nanoparticles existed in their metallic (Ag^0) state. Moreover, since the immobilization of AgNPs did not cause any shift in the peaks of ZnO nanorods, this immobilization strategy helps in depositing AgNPs without altering the crystalline behavior of the ZnO material.

X-ray photoelectron spectroscopy (XPS) analysis was performed to investigate the chemical states of Ag-ZnO hybrid nanorods (Fig. 3). The high resolution Zn 2p spectrum demonstrated two peaks at 1021.5 eV ($2p_{3/2}$) and 1044.5 eV ($2p_{1/2}$) which confirms the existence of zinc in Zn^{2+} form.³³ The high resolution Ag 3d spectrum of Ag-ZnO demonstrated two peaks at 367.5 eV ($\text{Ag } 3d_{5/2}$) and 373.5 eV ($\text{Ag } 3d_{3/2}$) with a peak splitting of 6.0 eV, which corresponds to metallic silver (Ag^0).⁷ Interestingly, the immobilization of AgNPs on ZnO template was evidenced through lowering in the binding energy values of 3d doublet as compared to their standard values in bulk silver *i.e.*, 368.2 eV and 374.2 eV, respectively.¹⁸ The reduction in charge density occurred due to the transfer of electrons from Ag to the conduction band of ZnO at the interface, creating a new fermi energy level for Ag-ZnO nanocomposite.^{18, 34} Similarly, peaks at 368.4 eV, 369.3 eV and 374.2 eV also suggest a strong association of silver with the oxygen and nitrogen moieties of arginine. A small fraction of these peaks can also be ascribed to $\text{AgO}/\text{Ag}_2\text{O}$ species due to the formation of a thin oxide layer over AgNPs while the immobilized nanoparticles predominantly exist in their Ag^0 oxidation state. The formation of oxide layer over AgNPs is inevitable under ambient conditions.³⁵ It is reported to facilitate controlled release of Ag^+ ions which enhances the biocidal performance.^{7, 36}

As predicted, the high resolution O 1s spectrum showed a relatively complex pattern due to various associations of oxygen atoms with zinc, oxygen, and arginine biomolecule and therefore, several possible peaks may coincide within a narrow range. The deconvoluted spectra showed peak at 530.2 eV which can be assigned to the lattice oxygen (O^{2-}) in ZnO.^{34, 37} A sharp peak at 531.3 eV provide sufficient indication of the Ag-O bond

formation in the hybrid nanocomposite, while a smaller proportion of $\text{AgO}/\text{Ag}_2\text{O}$ is also reported to exist within this region.⁷ The presence of arginine over ZnO nanorods was further confirmed through peaks at 532.9 eV which can be assigned to C-OH, C-O, and C=O bonds available for silver ions to bind with.³⁸ Beside this, the peak at 532-533 region is also attributed to the oxygen associated with the surface hydroxyl groups of ZnO.³³ There was also a small component peak of 535 eV which was ascribed to several associations of oxygen atom present in the arginine moieties.³⁹ Arginine being the only source of carbon and nitrogen, the appearance of carbon and nitrogen spectrum in the Ag/ZnO HNRs clearly indicates the existence of arginine over ZnO surface. The high resolution C 1s spectra was deconvoluted into three distinct peaks that correspond to C-C bond (285.7 eV), and the carbon atoms bonded to different functional moieties of arginine (C-O/C-N at 286.3 eV; and C=O/O-C=O at 290 eV).⁴⁰⁻⁴² Similarly, the N 1s spectra can be deconvoluted into three distinct peaks at 399.2 eV (C-N bond), 400.4 eV (C=N bond) and 400.7 eV (protonated amine, NH_3^+).⁴¹

Analyzing Ag/ZnO HNRs using FEG-SEM, it was noticed that ZnO nanorods were randomly aligned throughout the glass substrate, while AgNPs were observed as white dotted structures over the entire ZnO nanorods (Fig. 4a inset). A bunch of ZnO rods with immobilized AgNPs suggested that multiple nanorods may have grown from a single aggregate of ZnO seed during the growth process (Fig. 4b). The elemental composition of the sample was studied by energy-dispersive X-ray (EDX) analysis. As shown in Figure 4c (inset), the presence of zinc, oxygen and silver peaks appeared due to Ag/ZnO hybrid nanostructures, while a peak of silicon was observed because of the glass (silica) material used as the support matrix. A smaller proportion of arginine was also evidenced through a relatively smaller peak of carbon, whereas no nitrogen peak was identified due to insufficient element counts during the course of EDX analysis. The elemental mapping analysis for a selected region (indicated in pink) clearly showed that silver (green) is homogeneously distributed throughout the surface in addition to other major elements, *i.e.*, Zn (blue), O (white) and Si (red). Semi-quantitative estimation of the surface composition indicated that nearly 30% (by wt.) of the surface is occupied by elemental silver (See Table S1† in ESI). The absence of any other peaks clearly indicates that the synthesized antibacterial substrate is in pure form, thus validating an efficient immobilization of AgNPs using our greener approach.

Transmission electron microscopy (FEG-TEM) was performed to confirm the immobilization of AgNPs on ZnO surface (Fig. 5). Results obtained corroborate with that of the FEG-SEM analysis, where silver nanoparticles were found to be evenly distributed over ZnO nanorods (Fig. 5a). Analyzing the TEM micrographs of the ZnO surface (side view) it was evident that immobilized AgNPs were nearly spherical in shape with size ranged from 5-14 nm (Fig. 5b). The average size of AgNPs was found to be ~11 nm. HRTEM micrograph (Fig. 5c) reveals a distinct interface and spatial arrangement of atoms between AgNP and ZnO. The lattice fringes having d-spacing of 0.26 nm and 0.24 nm correspond to the crystallographic (002) plane of zinc and (111) plane of the face centred cubic AgNPs,³⁴ respectively (Fig. 5d-e). The selected area diffraction (SAED) analysis further validates the

presence of silver and zinc in Ag/ZnO HNRs due to their characteristic diffraction patterns.

Antibacterial Studies

It is worth mentioning that immobilizing AgNPs onto another bactericidal material, *i.e.*, ZnO may promote synergistic action and may cause superior antibacterial effect compared to AgNPs and ZnO each acting individually. In order to elucidate this, the antibacterial performances of three different antibacterial materials, *i.e.*, pure ZnO NRs, colloidal AgNPs (average size, 10 ± 2 nm), and AgNP-silica substrate were compared with Ag/ZnO HNRs against *E. coli* MTCC 443 strain at an initial cell count of 10^3 - 10^4 CFU ml⁻¹ in a 100 ml batch reactor. As shown in Figure 6a, the Ag/ZnO hybrid nanorods showed much faster antibacterial activity than pure ZnO nanorods and achieved 100% bactericidal activity in 30 minutes. In contrast to this, pure ZnO nanorods could not achieve complete bactericidal activity even after a much longer duration, *i.e.*, 120 minutes. Although the colloidal AgNPs showed promising bactericidal potential compared to the pure ZnO nanorods, the time to achieve complete disinfection was prolonged to 90 minutes. AgNP-silica substrate also demonstrated inferior bactericidal effect (50 minutes) than Ag/ZnO HNRs, which can be explained on the basis of ~ 3.5 higher silver loading in case of the latter. Analyzing these data, it can be predicted that the hybrid nanocomposite of AgNP and ZnO acts effectively against *E. coli* resulting in enhanced antibacterial performance compared to the individual components.

Zone of inhibition (ZoI) tests were performed to compare the bactericidal potential of the two substrates in solid medium (Fig. 6b). Results were in good agreement with that in the liquid medium where superior bactericidal activity of Ag/ZnO HNRs was marked by a noticeable ZoI formation. Pure ZnO NRs did not show a distinct inhibition zone. Fuchs and Tiller⁴³ demonstrated similar results where an antibacterial substrate depicted a distinct but narrow ZoI due to its contact-killing mechanism. The narrow width of the ZoI indicated that bacteria were able to grow in close proximity of the substrate since there was negligible release of biocidal material from the antibacterial substrate. Further, in order to verify its contact-killing bactericidal action, it was observed that the Ag/ZnO HNR-glass substrate not only killed bacterial colonies in that area but also suppressed further growth of bacteria at that zone even after 24-hour incubation, owing to its 'bacteriostatic' effect (see Fig. S2† in ESI). Similar photographic images have been shown in an earlier study,⁴⁴ where AgNP coated cellulose acetate fibers when placed in direct contact with bacterial lawn for 4 hours showed complete inhibition of *E. coli* growth at the contact area. Thus, it can be speculated that the Ag/ZnO HNRs mediate its antibacterial action majorly via contact-active mode. However, some diffusion of biocidal material from the immobilized substrate and its contribution towards antibacterial action cannot be ruled out.

Previous studies have demonstrated a substantial difference in bactericidal activity of antimicrobial material, if either the type of culture strain or the initial bacterial concentration is varied.^{7, 8, 26} To investigate the wide spectrum antibacterial activity of Ag/ZnO HNRs, *E. coli* MTCC 443 and *B. subtilis* MTCC 441 strains were selected as model Gram (-) and Gram (+) strains. Four independent tests were performed against each of the

strains, in deionized water (DI) and phosphate buffer medium (PBS), both at lower (10^3 CFU ml⁻¹) and higher (10^5 CFU ml⁻¹) initial cell concentration (Fig. 7). Ag/ZnO HNRs demonstrated good antibacterial activity against both types of strain where complete disinfection could be achieved within 70 minutes for all the test conditions. In DI water, it took 30 and 60 minutes for complete disinfection against *E. coli* at 10^3 and 10^5 CFU ml⁻¹ initial bacterial counts, respectively. Under similar test conditions, the time to achieve complete disinfection was marginally delayed to 40 and 70 minutes against *B. subtilis* strain, showing the strain-specific bactericidal activity of Ag/ZnO hybrid nanorods. As compared to DI water, no significant variation in the antibacterial activity of Ag/ZnO HNRs was observed in the phosphate buffer medium, which mimics physiological condition. Therefore, AgNP immobilized ZnO substrate can be well suited for other potential *in-vitro* applications, such as surgical coatings and wound dressings.

Antibacterial efficacy on multiple reuse

Nanocomposites, which act as immobilizing matrix and/or support for antibacterial agents are advantageous as they enable not only the convenient use of the antibacterial agents but also facilitate their release.⁵ However, the antibacterial activity of such materials is adversely affected due to the continuous depletion of Ag⁺ ions, rendering them unsuitable for long term use. One of the aims of the current study was to elucidate the antibacterial efficacy of Ag/ZnO HNRs on multiple reuse and to determine the corresponding silver and zinc release. As shown in Figure 8a, the Ag/ZnO HNRs remained bactericidal against *E. coli* MTCC 443 (10^3 CFU ml⁻¹) even after the same substrate was reused eleven times. Initially up to the 5th reuse, the time for complete killing remained constant at 30 minutes although the rate of kill was slower in the initial phase. For subsequent use, *i.e.*, 7th/9th and 11th reuse, the time to achieve complete disinfection using Ag/ZnO HNRs was increased by 5 and 10 minutes, respectively. Silver release after 90 minute duration for the 2nd, 4th, 6th, 8th, and 10th use was 103.8 ± 4.6 , 94.7 ± 2.5 , 65.2 ± 2.8 , 44.7 ± 2.5 , and 40 ± 1.1 ppb, respectively (Fig. 8b). As predicted, lowering in the disinfection kinetics can easily be explained on the basis of lower silver release with every subsequent use. Interestingly, as low as ~ 26 ppb (11th use, 30 min) of silver release was sufficient to elicit 100% killing of *E. coli* cells after multiple reuse. It was also essential to study whether the amount of Zn⁺² release from the ZnO nanorods over repeated use, contributed towards the enhanced bactericidal action of Ag/ZnO HNRs. Figure 8c shows that the amount of Zn release after 90 minutes was progressively reduced from 91.6 ± 2.4 ppb in 2nd use to 18.5 ± 0.2 ppb after 8th reuse. For subsequent uses, zinc release was not detected (below the detection limit). The variation in the release profile of silver and zinc in the aqueous phase can be explained on the basis of their different chemical state.¹⁹ Silver, present in their nanoparticulate form (Ag⁰) is considered to be more reactive than the oxide form of zinc (ZnO), which may lead to higher release of silver, both in the form of silver ions as well as AgNPs. Despite this, it was observed that the amount of silver and zinc release over 30 minute (*i.e.*, time for complete disinfection) with every use was well below the permissible concentration limits for Ag (*i.e.*, 100 ppb) and Zn (*i.e.*, 3-5 ppm) in potable water, as defined by world health organization.²⁰ Therefore, it can be predicted that

the Ag/ZnO HNRs would pose minimum health risks. Low discharge of the biocidal materials would also minimize adverse effects on other organisms in the ecosystem.

The disinfection profile and silver/zinc release profiles on multiple reuse also gave useful insights to determine the mechanism of antibacterial action of Ag/ZnO HNRs. As the results indicated, the continuous depletion of silver and zinc ions did not significantly affect the extent of disinfection with every usage. This implies that the mode of bactericidal action of Ag/ZnO HNRs cannot be fully explained on the basis of release of silver and zinc only. Rather, the immobilized Ag/ZnO HNRs may act primarily through a contact-killing mode. In our recent study,⁷ it was illustrated that immobilized AgNPs demonstrated bactericidal action predominately via direct contact-killing mode, while release of silver ions had a minimum role on disinfection. In this study, the extent of disinfection remained the same irrespective of significant reduction (~37%) in silver release after the 2nd to 6th reuse, indicating the role of direct contact in bacterial killing. Interestingly, release of zinc ions appeared to have no significant contribution on the bactericidal performance since there was only a marginal delay in achieving complete disinfection after the 10th reuse, where zinc release was not even detected. This showed that Ag/ZnO HNRs could retain its antibacterial efficacy and was unaffected by the absence of zinc ions in the releasing media. These results preclude our initial hypothesis regarding the synergistic role of zinc and silver nanoparticles in the antibacterial action of Ag/ZnO HNRs. In contrast to this, the ZnO template seems to contribute primarily by providing a high surface area for deposition of AgNPs, thereby facilitating the direct-contact mode of action of immobilized AgNPs. Therefore, the enhanced antibacterial action of Ag/ZnO substrate can be better described by dual mode of bactericidal action, *i.e.*, direct contact killing upon contact of bacteria with Ag/ZnO HNRs and leaching of silver in nanoparticulate and/or ionic form.

***E. coli*-Ag/ZnO interaction**

In order to further investigate the interaction behaviour of AgNP/ZnO substrate with the bacterial cells, SEM and TEM imaging were done (Fig. 9). Ag/ZnO HNR treated *E. coli* cells showed adverse effects as compared to the untreated cells (see Fig. S3a† in ESI), and significant population of AgNPs were observed inside the bacterial cells (Fig. 9a). The presence of AgNPs near the cell membrane and inside the cells is considered to be the most fundamental and accepted mechanism for the antibacterial action of AgNPs other than silver ions release.^{46, 47} AgNPs were located both at, the periphery of the cell membrane as well as deep within the cells as aggregates with a peculiar pattern (Fig. 9b). Similar pattern of AgNP aggregates have been evidenced in an earlier study, where the role of bacterial surface proteins was found to be critical for AgNP binding and aggregation pattern formation.⁴⁸ Therefore, it can be hypothesized that during earlier stages of bacteria-AgNP interaction, the presence of surface proteins facilitated the formation of AgNP aggregates and mediated their subsequent entry into the intracellular environment via endocytosis (Fig. 9c). After successful internalization, AgNP aggregates could be translocated inside the bacterial machinery to carry out antibacterial action through multiple mechanisms, such as ROS

generation, blocking cell respiration and inhibiting DNA replication. These mechanisms may work concurrently and mediate enhanced antibacterial effect. While assessing the Ag/ZnO- *E. coli* interactions, the presence of crystalline form (Fig. 9e) and appearance of the characteristic peak at ~2.9 kV during EDX analysis (see, Fig. S3b† in ESI) supported the existence of AgNPs (*i.e.*, Ag⁰) in bacterial cells. In contrast to this, crystalline Zn was not detected in any of the treated bacterial cells. Thus, its role in antibacterial action was not mediated via zinc nanoparticles. The release studies have also shown negligible role of zinc ions. The antibacterial action was mediated by silver both in the form of AgNPs and silver ions.

Based on FEG-SEM analysis, some other possible mechanisms of bactericidal action may be hypothesized. As shown in the micrograph (Fig. 9e), Ag/ZnO HNR treated cells appeared to depict atypical shape and a few of the cells were severely damaged (encircled). Membrane disruption may increase the cell permeability and allow intracellular material to come out, ultimately causing cell death (Fig. 9e, inset above).⁴⁹ The formation of pits and holes on the bacterial surface indicates cell damage which consequently allows the internalization of AgNPs (Fig. 9e, inset below).²⁶ We also observed that AgNPs were not only present inside the bacterial cells, there were universally present over the entire bacterial surface (Fig. 9f). The interaction of AgNP/ZnO with bacterial cells leads to multiple pathways for bactericidal action, where it is extremely difficult to analyze which mechanism predominates over another. It can be assumed that an initial AgNP-bacterial interaction plays an important role. The results clearly indicate that the hybrid nanocomposite containing AgNPs and ZnO is a promising candidate for antibacterial applications owing to its dual mode of antibacterial action, contact-killing and release of metal ions.

Cytotoxicity analysis on human HepG2 cells

Use of nanomaterials containing silver and zinc oxide is often limited for therapeutic purposes owing to their intrinsic cytotoxic effects on humans.⁵⁰ A few recent studies have shown that the immobilization of AgNPs onto a substrate matrix would limit the release of silver in aqueous medium thereby, pose either minimal toxic effects or none at all on mammalian cells.⁵¹⁻⁵⁴ Agarwal *et al.*⁵¹ demonstrated that AgNPs immobilized on a polyelectrolyte multilayer (PEMs) films of poly(allylamine hydrochloride) and poly(acrylic acid) did not induce any cytotoxic effects against mouse fibroblast cell line, NIH-3T3 under various test conditions. Beside this, AgNP-impregnated PEMs showed good antibacterial activity against *Staphylococcus epidermidis*, a clinical isolate from veterinary hospital. In a different study, poly(L-glutamic acid)-capped silver nanoparticles were encapsulated within poly(lactide-co-glycolide) nanoparticles, which showed superior antibacterial activity against seven pathogenic strains without affecting cell viability of the human HepG2 cells.⁵⁴ Therefore, it is quite possible to construct non-cytotoxic, AgNP-based antibacterial substrates by exploring some effective immobilization strategies, which can control silver release into the medium to an amount, just sufficient to cause bactericidal effects.

In order to establish the fact that Ag/ZnO HNRs exhibit an enhanced, long-term antibacterial efficacy and do not pose undesirable toxic implications on human cells, cytotoxicity

experiments were performed against HepG2 cells through MTT assay. HepG2 cells are considered to be a useful *in-vitro* model for the detection of cytotoxic and genotoxic agents.⁵⁵ As shown in Figure 10a, cell viability of HepG2 cells treated with Ag/ZnO-25 HNRs were tested at four different time periods, *i.e.*, 6, 12, 24 and 48 hours. Compared to untreated cells (negative control), cells treated with Ag/ZnO HNR did not show any significant reduction in cell viability even after 24 hours of incubation. Pristine glass substrate did not contribute towards any cytotoxic effects and showed similar cell viability as with the Ag/ZnO HNRs. As a positive control for toxicity, cells treated with Triton-X 100 showed complete absence of cell viability. Under the given test conditions, Ag/ZnO HNRs showed no cytotoxic effects on human cells, which is indicative of good biocompatibility of the hybrid nanocomposite. Moreover, we can interpret its minimal toxicological consequences on aquatic organisms, due to low discharge of silver and zinc from the immobilizing template. The silver loading in Ag/ZnO HNRs ($1 \times 1 \text{ cm}^2$) was calculated to be $2.8 \mu\text{g cm}^{-2}$, which is nearly ~ 10 fold lower ($25 \mu\text{g cm}^{-2}$) than that reported by Shi *et al.*⁵³ where AgNPs were immobilized on PEMS functionalized stainless steel surface. Even at a much higher AgNP loading, Shi *et al.*⁵³ did not find any cytotoxic effects on mammalian cells. Thus, Ag/ZnO HNRs do not provoke cytotoxic responses to human cells and yet demonstrated excellent antibacterial efficacy.

A number of studies have proposed sub-lethal effects of AgNPs and nano-ZnO, when present either in very low concentration or short incubation times,^{56, 57} due to the generation of intracellular reactive oxygen species (ROS). Higher production of intracellular ROS can induce severe oxidative stress and is considered to be one of the most important mechanisms for cellular apoptosis, due to nanomaterial exposure.⁵⁸ To determine whether the interaction between Ag/ZnO hybrid nanorods and HepG2 cells would lead to oxidative stress, we measured the intracellular ROS generation using the DCFDA assay. As shown in Figure 10b, no significant increment in ROS generation was noticed up to 24 hours, as compared to the untreated cells. A relatively longer period of treatment (*i.e.*, 48 hours) may pose some sub-toxic effects to cells, as indicated by a slight increase in the ROS level. The positive control, tertiary butyl hydroperoxide (t-BH) induced a 3.2 fold increase in ROS generation as compared to the untreated cells. These results are in contrast to earlier studies, where AgNPs and ZnO nanoparticles have been reported to induce severe oxidative stress to cells both, by their “nanoparticulate” effect as well as release of ionic forms.⁵⁹⁻⁶² It was therefore anticipated that probably the intrinsic chemical composition of Ag/ZnO hybrid nanorods could have inhibitory effect on ROS generation. Interestingly, L-arginine, one of the component of Ag/ZnO HNR synthesized in this study has been reported to act as a free radical scavenger and possesses antioxidant properties.⁶³ Tripathi *et al.*⁶⁴ also reported use of L-arginine as an oral supplement to patients suffering from acute myocardial infarction, as it retards ROS production by scavenging the oxygen derived free radicals. Stevanovic *et al.*⁵⁴ have recently demonstrated the ROS scavenging property of ascorbic acid, another antioxidant molecule whose presence made the AgNP-loaded material to be highly bactericidal without posing cytotoxic effects on HepG2 cells. Therefore, it is expected

that the presence of arginine not only facilitated dense immobilization of AgNPs on ZnO nanorods, it could also inhibit the ROS-induced cytotoxicity to some extent. Further tests will be required to determine their sub-lethal, genotoxic effects in detail.

4. Conclusions

In this study, we have demonstrated a facile, inexpensive and entirely green approach for immobilization of silver nanoparticle on ZnO nano template. The presence of arginine not only facilitates a high localized assembly of AgNPs, it also enhances the stability of ZnO deposition on the glass matrix and reduces the potential toxicity by limiting the release of zinc ions under the alkaline conditions. The Ag/ZnO hybrid nanomaterial was found to be extremely stable in aqueous medium and showed an extraordinary bactericidal effect against both Gram-positive and Gram-negative bacterial strains. The results obtained through zone of inhibition (ZoI) studies and surface contact tests also depict growth inhibition of bacterial cells (*i.e.*, bacteriostatic effect). The Ag/ZnO HNRs acted primarily through direct contact killing mode and released very low concentration of silver and zinc in the aqueous media, thus minimizing potential health risks and other adverse effects associated with their discharge. Cytotoxicity results clearly indicate that Ag/ZnO HNRs deposited on glass substrates do not induce cytotoxic effects on human cell line, but retain antibacterial efficacy even after multiple reuse. This immobilization strategy therefore holds good promise and enormous potential to be exploited for various antibacterial coatings in implantable biomaterials and surgical instruments.

Acknowledgements

The authors gratefully acknowledge Sophisticated Analytical Instrument Facility (SAIF), and IIT-Bombay central facility (XRD, ICP-AES, XPS and FEG-TEM) for characterization studies. We also acknowledge Department of Chemical Engineering, IIT Bombay for BET measurement test. This study was partially funded by Nanomission, DST, Govt. of India.

Notes

⁹⁵ ^aCentre for Research in Nanotechnology and Science, Indian Institute of Technology-Bombay, Powai, Mumbai 400076, India

^bCentre for Environmental Science and Engineering, Indian Institute of Technology-Bombay, Powai, Mumbai 400076, India

^cDepartment of Biosciences and Bioengineering, Indian Institute of Technology-Bombay, Powai, Mumbai 400076, India

^dCentre of Excellence in Nanoelectronics, Indian Institute of Technology-Bombay, Powai, Mumbai 400076, India E.mail: mukherji@iitb.ac.in; Tel: 091-22-2576-7767; Fax: 091-22-2572 3480

¹⁰⁵ † Electronic Supplementary Information (ESI) available: [synthesis of ZnO nanorods, instrumentation details, contact killing of Ag/ZnO]. See DOI: 10.1039/b000000x/

References

1. S. Chernousova and M. Epple, *Angew. Chem. Int. Edit.*, 2013, **52**, 1636.

2. M. J. Hajipour, K. M. Fromm, A. Akbar Ashkarran, D. Jimenez de Aberasturi, I. R. d. Larramendi, T. Rojo, V. Serpooshan, W. J. Parak and M. Mahmoudi, *Trends Biotechnol.*, 2012, **30**, 499.
3. A. Ivask, A. ElBadawy, C. Kaweeteerawat, D. Boren, H. Fischer, Z. Ji, C. H. Chang, R. Liu, T. Tolaymat, D. Telesca, J. I. Zink, Y. Cohen, P. A. Holden and H. A. Godwin, *ACS Nano*, 2013, **8**, 374.
4. Q. H. Tran and A. T. Le, *Adv. Nat. Sci.: Nanosci. Nanotechnol.*, 2013, **4**, 033001.
5. M. Lv, S. Su, Y. He, Q. Huang, W. Hu, D. Li, C. Fan and S. T. Lee, *Adv. Mater.*, 2010, **22**, 5463.
6. C. Tang, W. Sun and W. Yan, *RSC Advances*, 2014, **4**, 523.
7. S. Agnihotri, S. Mukherji and S. Mukherji, *Nanoscale*, 2013, **5**, 7328.
8. S. Mukherji, J. Ruparelia and S. Agnihotri, in *Nano-Antimicrobials: Progress and Prospects*, ed. N. Cioffi and M. Rai, Springer-Verlag Berlin Heidelberg, 2012, pp. 225.
9. S. Agnihotri, S. Mukherji and S. Mukherji, *Appl. Nanosci.*, 2012, **2**, 179.
10. N. Perkas, G. Amirian, G. Applerot, E. Efendiev, Y. Kaganovskii, A. V. Ghule, B. J. Chen, Y. C. Ling and A. Gedanken, *Nanotechnology*, 2008, **19**, 435604.
11. M. Moritz and M. Geszke-Moritz, *Chem. Eng. J.*, 2013, **228**, 596.
12. P. Dallas, J. Tucek, D. Jancik, M. Kolar, A. Panacek and R. Zboril, *Adv. Funct. Mater.*, 2010, **20**, 2347.
13. Z. Li, H. Tang, W. Yuan, W. Song, Y. Niu, L. Yan, M. Yu, M. Dai, S. Feng and M. Wang, *Nanotechnology*, 2014, **25**, 145702.
14. I. Ocoy, M. L. Paret, M. A. Ocoy, S. Kunwar, T. Chen, M. You and W. Tan, *ACS Nano*, 2013, **7**, 8972.
15. K. R. Raghupathi, R. T. Koodali and A. C. Manna, *Langmuir*, 2011, **27**, 4020.
16. Y. Zhang, X. Gao, L. Zhi, X. Liu, W. Jiang, Y. Sun and J. Yang, *J. Inorg. Biochem.*, 2014, **130**, 74.
17. W. Lu, G. Liu, S. Gao, S. Xing and J. Wang, *Nanotechnology*, 2008, **19**, 445711.
18. Q. Deng, X. Duan, D. H. Ng, H. Tang, Y. Yang, M. Kong, Z. Wu, W. Cai and G. Wang, *ACS Appl. Mater. Interfaces*, 2012, **4**, 6030.
19. S. Jaiswal, P. McHale and B. Duffy, *Colloids Surf., B*, 2012, **94**, 170.
20. S. C. Motshekga, S. S. Ray, M. S. Onyango and M. N. Momba, *J. Hazard. Mater.*, 2013, **262**, 439.
21. T. Siva Vijayakumar, S. Karthikeyeni, S. Vasanth, A. Ganesh, G. Bupesh, R. Ramesh, M. Manimegalai and P. Subramanian, *J. Nanosci.*, 2013, **7**.
22. T. Shoeib, K. M. Siu and A. C. Hopkinson, *J. Phys. Chem. A*, 2002, **106**, 6121.
23. Y. W. Heo, S. J. Pearton, D. P. Norton and F. Ren, *Semiconductor device-based sensors for gas, chemical, and biomedical applications*, CRC Press, 2011.
24. C. K. Thai, H. Dai, M. Sastry, M. Sarikaya, D. T. Schwartz and F. Baneyx, *Biotechnol. Bioeng.*, 2004, **87**, 129.
25. A. Legler, A. Kazachenko, V. Kazbanov, O. Per'yanova and O. Veselova, *Pharm. Chem. J.*, 2001, **35**, 501.
26. S. Agnihotri, S. Mukherji and S. Mukherji, *RSC Advances*, 2014, **4**, 3974.
27. S. Mohanty, S. Mishra, P. Jena, B. Jacob, B. Sarkar and A. Sonawane, *Nanomed-Nanotechnol.*, 2012, **8**, 916.
28. M. W. Forbes, M. F. Bush, N. C. Polfer, J. Oomens, R. C. Dunbar, E. R. Williams and R. A. Jockusch, *J. Phys. Chem. A*, 2007, **111**, 11759.
29. A. Aliaga, C. Garrido, P. Leyton, G. Diaz F, J. S. Gomez-Jeria, T. Aguayo, E. Clavijo, M. Campos-Vallette and S. Sanchez-Cortes, *Spectrochim. Acta, Part A*, 2010, **76**, 458.
30. C. Garrido, T. Aguayo, E. Clavijo, J. Gómez-Jeria and M. Campos-Vallette, *J. Raman Spectrosc.*, 2013, **44**, 1105.
31. S. K. Das, M. M. R. Khan, A. K. Guha and N. Naskar, *Green Chem.*, 2013, **15**, 2548.
32. W. Xie, Y. Li, W. Sun, J. Huang, H. Xie and X. Zhao, *J. Photochem. Photobiol., A*, 2010, **216**, 149.
33. S. Ghosh, V. Goudar, K. Padmalekha, S. Bhat, S. Indi and H. Vasana, *RSC Advances*, 2012, **2**, 930.
34. S. A. Ansari, M. M. Khan, M. O. Ansari, J. Lee and M. H. Cho, *J. Phys. Chem. C*, 2013, **117**, 27023.
35. M. Schmidt, A. Masson and C. Brechignac, *Phys. Rev. Lett.*, 2003, **91**, 243401.
36. G. A. Sotiriou, A. Meyer, J. T. Knijnenburg, S. Panke and S. E. Pratsinis, *Langmuir*, 2012, **28**, 15929.
37. P. Prieto, V. Nistor, K. Nouneh, M. Oyama, M. Abd-Lefdil and R. Diaz, *Appl. Surf. Sci.*, 2012, **258**, 8807.
38. Y. Chi, L. Zhao, Q. Yuan, X. Yan, Y. Li, N. Li and X. Li, *J. Mater. Chem.*, 2012, **22**, 13571.
39. S. Song, B. You, Y. Zhu, Y. Lin, Y. Wu and X. Ge, *Cryst. Growth Des.*, 2014, **14**, 38.
40. V. Datsyuk, M. Kalyva, K. Papagelis, J. Parthenios, D. Tasis, A. Siokou, I. Kallitsis and C. Galiotis, *Carbon*, 2008, **46**, 833.
41. H. J. Kim, I.-S. Bae, S.-J. Cho, J.-H. Boo, B.-C. Lee, J. Heo, I. Chung and B. Hong, *Nanoscale Res. Lett.*, 2012, **7**, 1.
42. B. Xia, S. J. Xiao, D. J. Guo, J. Wang, J. Chao, H. B. Liu, J. Pei, Y. Q. Chen, Y. C. Tang and J. N. Liu, *J. Mater. Chem.*, 2006, **16**, 570.
43. A. D. Fuchs and J. C. Tiller, *Angew. Chem. Int. Edit.*, 2006, **45**, 6759.
44. F. Cheng, J. W. Betts, S. M. Kelly, J. Schaller and T. Heinze, *Green Chem.*, 2013, **15**, 989.
45. J. P. Ruparelia, A. K. Chatterjee, S. P. Duttagupta and S. Mukherji, *Acta Biomater.*, 2008, **4**, 707.
46. M. Auffan, J. Rose, J. Y. Bottero, G. V. Lowry, J. P. Jolivet and M. R. Wiesner, *Nat. Nanotechnol.*, 2009, **4**, 634.
47. J. R. Morones, J. L. Elechiguerra, A. Camacho, K. Holt, J. B. Kouri, J. T. Ramirez and M. J. Yacaman, *Nanotechnology*, 2005, **16**, 2346.
48. S. C. Hayden, G. Zhao, K. Saha, R. L. Phillips, X. Li, O. R. Miranda, V. M. Rotello, M. A. El-Sayed, I. Schmidt-Krey and U. H. Bunz, *J. Am. Chem. Soc.*, 2012, **134**, 6920.
49. I. Sondi and B. Salopek-Sondi, *J. Colloid Interface Sci.*, 2004, **275**, 177.
50. O. Bondarenko, K. Juganson, A. Ivask, K. Kasemets, M. Mortimer and A. Kahru, *Arch. Toxicol.*, 2013, **87**, 1181.
51. A. Agarwal, T. L. Weis, M. J. Schurr, N. G. Faith, C. J. Czuprynski, J. F. McAnulty, C. J. Murphy and N. L. Abbott, *Biomaterials*, 2010, **31**, 680.
52. C. Y. Chu, F. C. Peng, Y. F. Chiu, H. C. Lee, C. W. Chen, J. C. Wei and J. J. Lin, *PLOS One*, 2012, **7**, e38360.
53. Z. Shi, K. Neoh, S. Zhong, L. Yung, E. Kang and W. Wang, *J. Biomed. Mater. Res., Part A*, 2006, **76**, 826.
54. M. Stevanović, I. Bračko, M. Milenković, N. Filipović, J. Nunić, M. Filipič and D. P. Uskoković, *Acta Biomater.*, 2014, **10**, 151.
55. V. Mersch-Sundermann, S. Knasmüller, X.-j. Wu, F. Darroudi and F. Kassie, *Toxicology*, 2004, **198**, 329.

-
56. C. Carlson, S. Hussain, A. Schrand, L. K. Braydich-Stolle, K. Hess, R. Jones and J. Schlager, *J. Phys. Chem. B*, 2008, **112**, 13608.
57. M. J. Piao, K. A. Kang, I. K. Lee, H. S. Kim, S. Kim, J. Y. Choi, J. Choi and J. W. Hyun, *Toxicol. Lett.*, 2011, **201**, 92.
58. A. Nel, T. Xia, L. Mädler and N. Li, *Science*, 2006, **311**, 622.
59. J. Fabrega, S. R. Fawcett, J. C. Renshaw and J. R. Lead, *Environ. Sci. Technol.*, 2009, **43**, 7285.
60. E. Navarro, F. Piccapietra, B. Wagner, F. Marconi, R. Kaegi, N. Odzak, L. Sigg and R. Behra, *Environ. Sci. Technol.*, 2008, **42**, 8959.
61. Z. M. Xiu, Q. B. Zhang, H. L. Puppala, V. L. Colvin and P. J. J. Alvarez, *Nano Lett.*, 2012, **12**, 4271.
62. X. Yang, A. P. Gondikas, S. M. Marinakos, M. Auffan, J. Liu, H. Hsu-Kim and J. N. Meyer, *Environ. Sci. Technol.*, 2011, **46**, 1119.
63. A. Lass, A. Suessenbacher, G. Wolkart, B. Mayer and F. Brunner, *Mol. Pharmacol.*, 2002, **61**, 1081.
64. P. Tripathi, T. P. Singh, M. Chandra and M. K. Misra, *Int. J. Biol. Medical Res.*, 2010, **1**, 15.

20

Cite this: DOI: 10.1039/c0xx00000x

www.rsc.org/xxxxxx

FULL PAPER

List of Figures

Fig. 1 Schematic representation of in-situ synthesis and immobilization of silver nanoparticles on ZnO nanorods using arginine as a linker

Fig. 2 UV-Vis extinction spectroscopy (a) and X-ray diffraction analysis (b) of pure ZnO and AgNP immobilized ZnO hybrid nanorods (HNRs)

Fig. 3 XPS spectral analysis of Ag/ZnO hybrid nanorods showing full scan and corresponding deconvoluted peaks in the high resolution (HR) spectra of various elements present, *i.e.*, Zn (2p), Ag (3d), O (1s), C (1s), and N(1s)

Fig. 4 FEG-SEM micrographs showing (a) uniform deposition of Ag/ZnO nanorods on the glass substrate. Image in the inset reveals a high deposition of silver nanoparticles. (b) Bunch of ZnO nanorods with immobilized AgNPs (c) Elemental mapping done for the selected region revealed the presence of zinc (Zn, blue), oxygen (O, white), silver (Ag, green) and silicon (Si, red). Surface composition of the substrate was based on EDX analysis, with characteristic peak of silver at ~2.9 kV in addition to other elements

Fig. 5 FEG-TEM micrograph of (a) a single ZnO nanorod with uniform immobilization of silver nanoparticles. (b) Side view of Ag/ZnO nanorods and immobilized AgNP at the tip of ZnO (inset). HRTEM image (c) showing a distinct interface between Ag and ZnO. High resolution micrographs of ZnO (d) and silver nanoparticles (e) with characteristic d-spacing and corresponding diffraction patterns of ZnO (above panel) and silver (below panel) are also presented

Fig. 6 (a) Comparative disinfection potential of pure ZnO nanorods, AgNP immobilized ZnO nanorods (Ag/ZnO HNRs) and colloidal AgNPs (12 ± 2 nm, 6.0×10^{-2} mg in mass). All disinfection studies were performed using *E. coli* MTCC 443 strain (initial cell concentration, $\sim 10^3$ CFU ml⁻¹) in a 100 ml batch reactor. (b) Zone of inhibition (ZoI) tests done at relatively higher bacterial counts (10^5 - 10^6 CFU ml⁻¹) showing the bacteriostatic effect of Ag/ZnO HNRs while no ZoI was observed in case with pure ZnO nanorods

Fig. 7 Strain-specific antibacterial activity of Ag/ZnO hybrid nanorods (2×2.3 cm²) against (a) Gram-negative, *E. coli* MTCC 443 and (b) Gram-positive, *B. subtilis* MTCC 441 strain. For each strain, disinfection kinetics was tested at an initial concentration of 10^3 CFU ml⁻¹ (triangle) and 10^5 CFU ml⁻¹ (square) in both, deionized water (continuous line) and phosphate buffer medium (dashed line)

Fig. 8 (a) Disinfection performance of a single Ag/ZnO HNR substrate ($2 \times 2.3 \text{ cm}^2$) after 11 times repeated usage against *E. coli* MTCC 443 (10^3 CFU ml^{-1}). (b) Corresponding silver release profile (b) after every usage was evaluated. (c) Zinc release after each use over 30 min and 90 minute duration. (# below the detection limit)

Fig. 9 FEG-TEM (a-e) and FEG-SEM (f-g) analyses of *E. coli* cells (bacterial count, 10^6 - 10^7 CFU ml^{-1}) treated with Ag/ZnO HNR loaded substrate. (a) Lower and (b) higher magnification showing the presence of AgNPs, both near the cell membrane and in the interiors of bacterial cells. (c) An early and (d) late stage of internalization of AgNP aggregates (white arrow) near the cell membrane (black arrow). (e) Crystalline structure reveals the presence of silver in its Ag^0 state, *i.e.*, AgNPs. SEM images of (f) damaged *E. coli* cells with ruptured morphology (inset, above) and formation of pits and holes on the bacterial surface (inset, below). (g) Silver nanoparticles were homogeneously present all over the surface of bacterial cells

Fig. 10 Cytotoxicity analysis of Ag/ZnO hybrid nanorods on human hepatocarcinoma (HepG2) cells as determined by (a) MTT assay and (b) intracellular ROS generation. Cells were treated with Ag/ZnO HNRs deposited on glass substrate ($1 \times 1 \text{ cm}^2$) and pristine glass substrate ($1 \times 1 \text{ cm}^2$) for various time periods and (a) percentage of cells viability (b) intracellular ROS level was evaluated after each treatment. Triton X-100 and tertiary butyl hydroperoxide (t-BH) were taken as positive control for MTT and ROS determination experiments, respectively. Experiments were performed in triplicate; data shown are expressed as mean \pm standard error

20

25

30

35

40

45

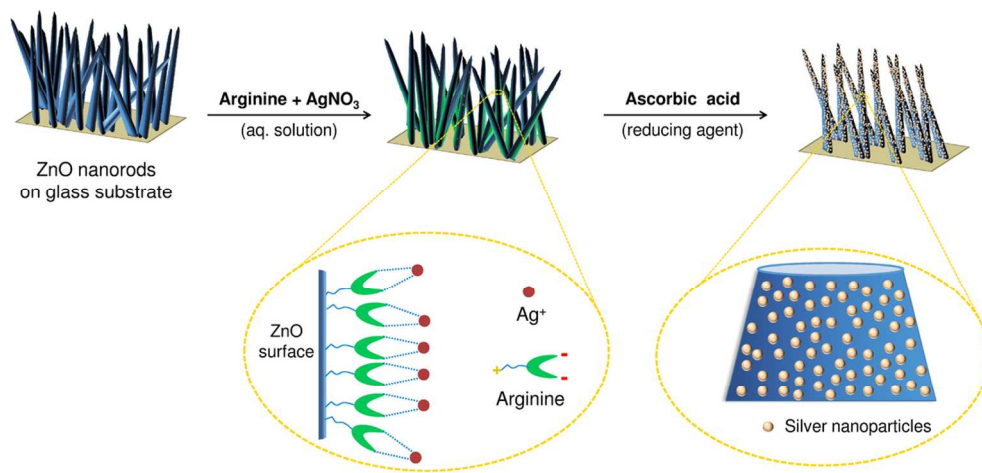
50

List of Table

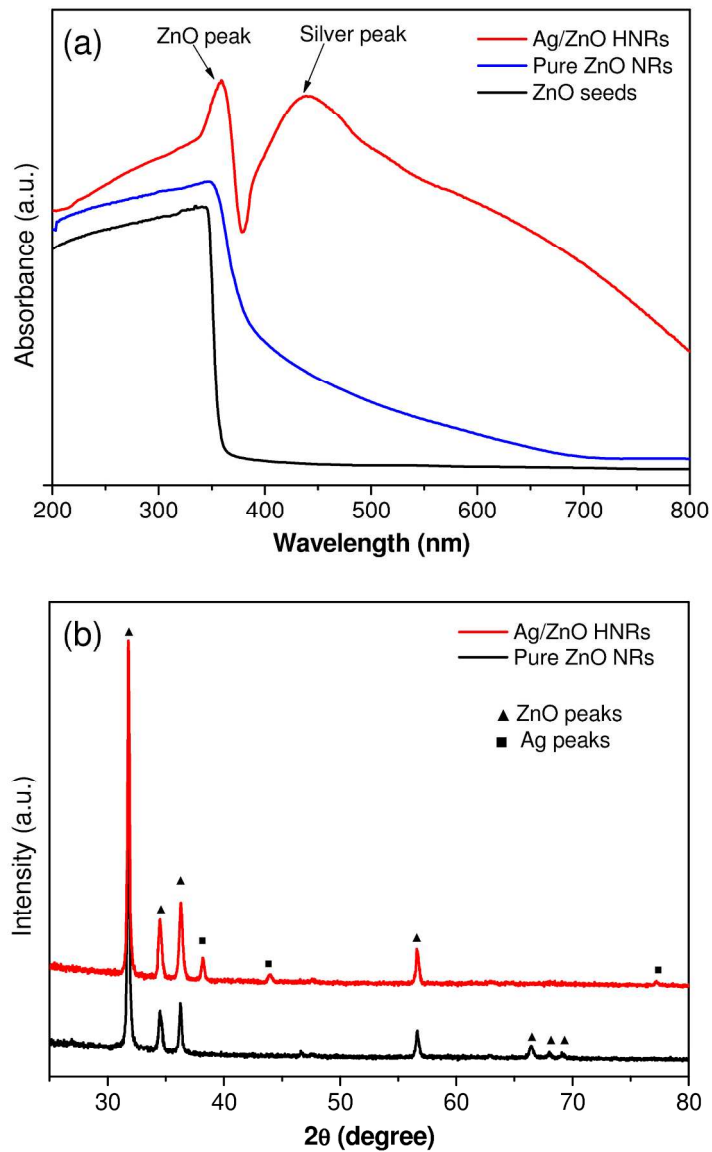
⁵
Table 1. ICP-AES analysis of ZnO nanorods loaded with various amount of silver nanoparticles

Sample code	Zn content* (μg)	Ag content* (μg)	Ag : Zn	Ag loading ($\mu\text{g cm}^{-2}$)
Pure ZnO	974 \pm 55	0.0	0.000	0.00
Ag/ZnO-5	938 \pm 61	8.1 \pm 0	0.009 \pm 5.4 x 10 ⁻⁵	1.76
Ag/ZnO-10	959 \pm 35	19.3 \pm 3	0.020 \pm 7.2 x 10 ⁻⁴	4.20
AgZnO-20	1016 \pm 91	59.0 \pm 5	0.058 \pm 1.2 x 10 ⁻³	12.83
Ag/ZnO-25	1019 \pm 36	31.2 \pm 6	0.031 \pm 1.6 x 10 ⁻³	6.79
Ag/ZnO-75	964 \pm 93	16.2 \pm 2	0.017 \pm 5.9 x 10 ⁻⁴	3.52

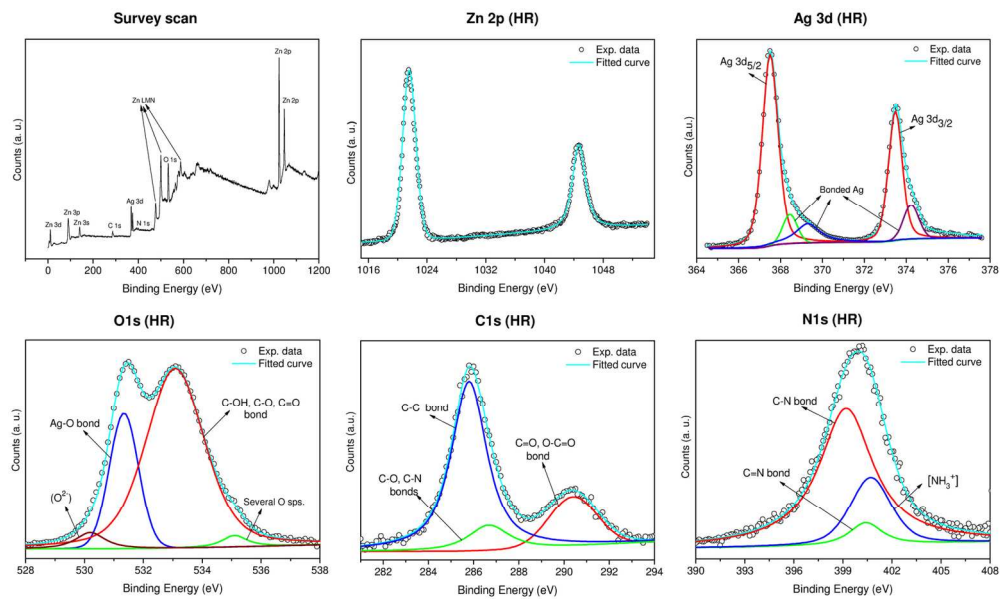
*Average values based on three independent tests



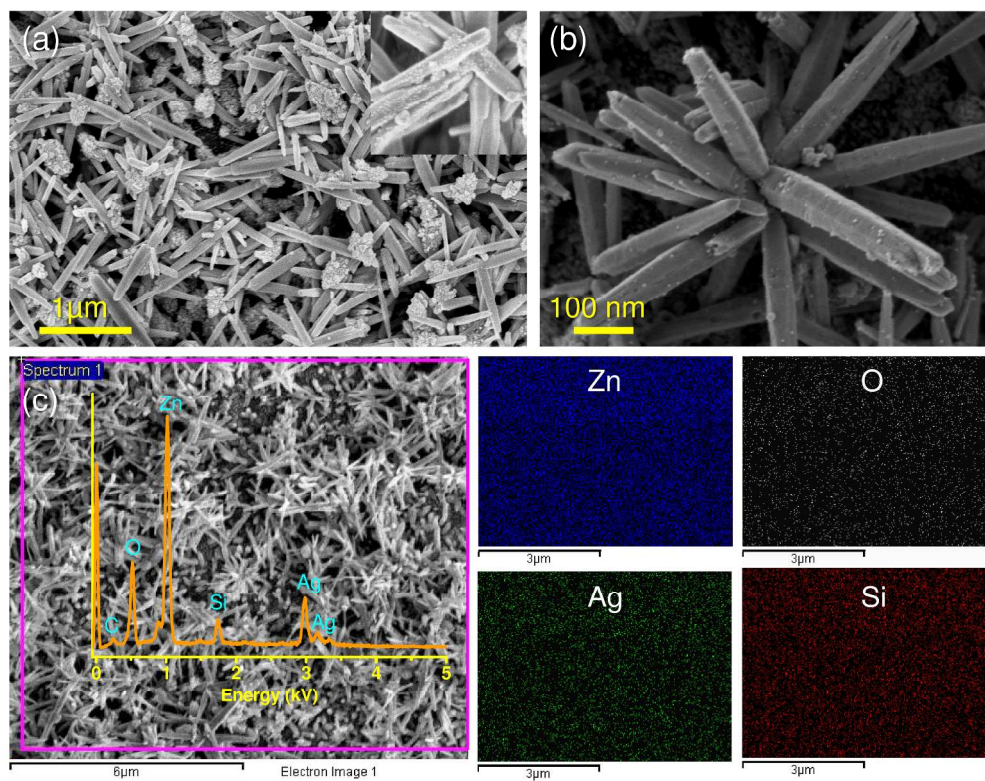
Schematic representation of *in-situ* synthesis and immobilization of silver nanoparticles on ZnO nanorods using arginine as a linker
109x53mm (300 x 300 DPI)



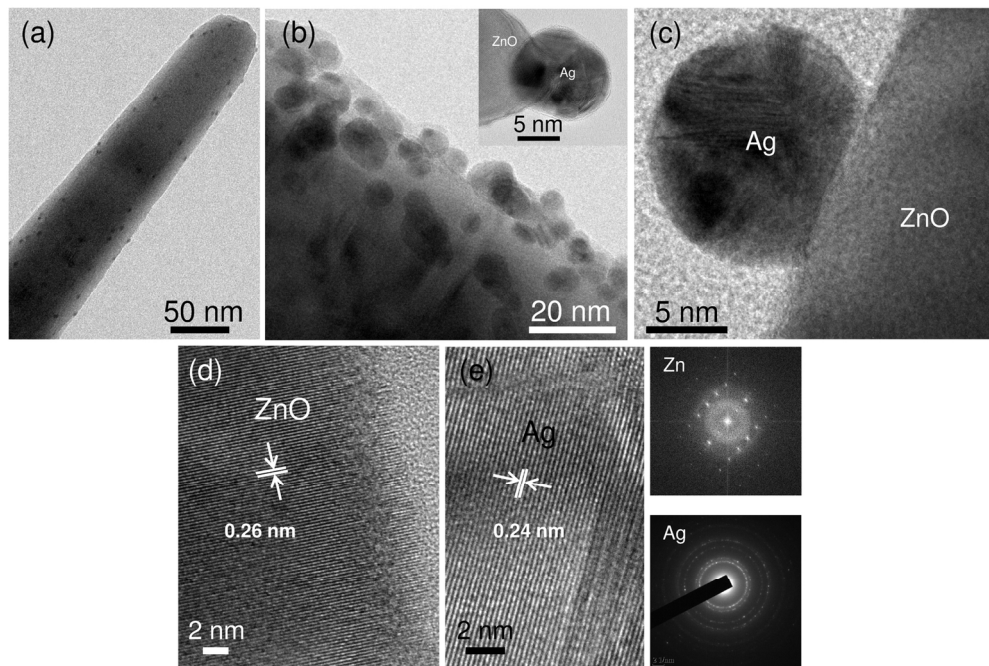
UV-Vis extinction spectroscopy (a) and X-ray diffraction analysis (b) of pure ZnO and AgNP immobilized ZnO hybrid nanorods (HNRs)
175x273mm (300 x 300 DPI)



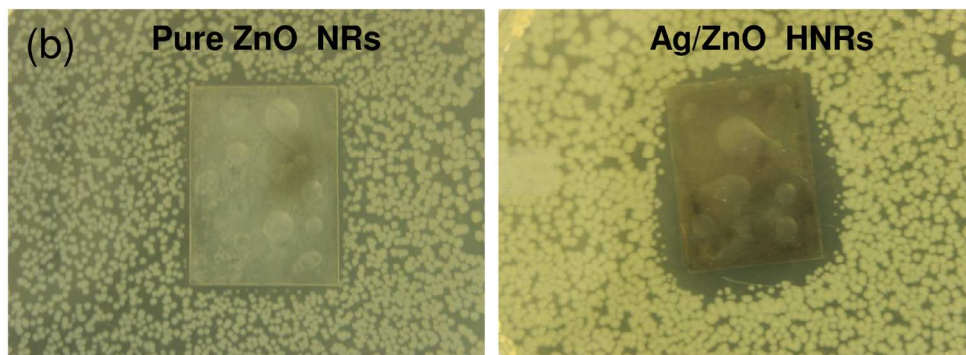
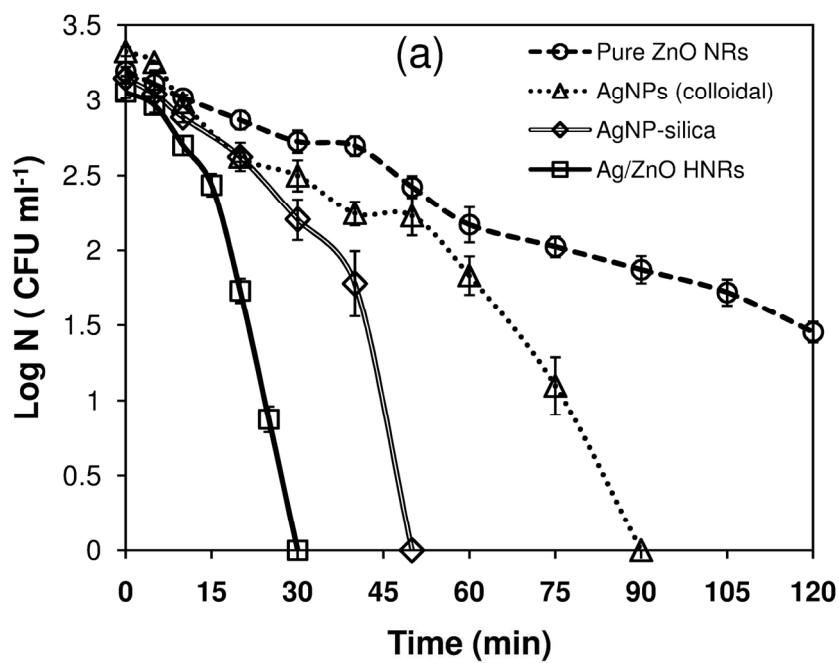
XPS spectral analysis of Ag/ZnO hybrid nanorods showing full scan and corresponding deconvoluted peaks in the high resolution (HR) spectra of various elements present, *i. e.*, Zn(2p), Ag(3d), O(1s), C(1s), and N(1s) 148x89mm (300 x 300 DPI)



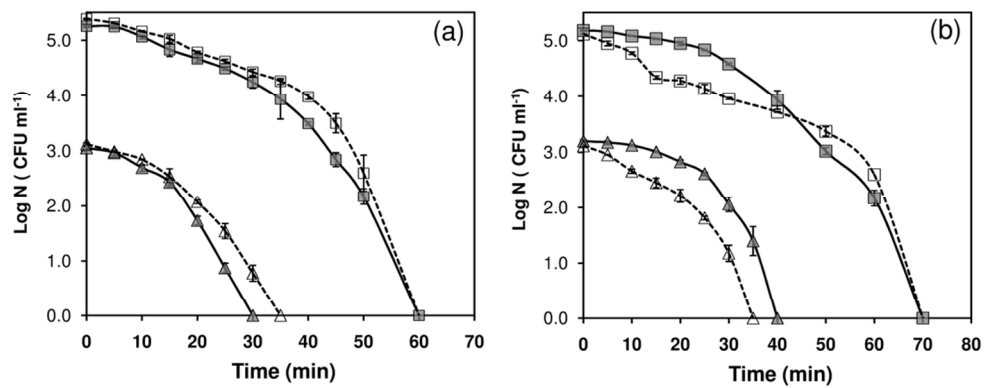
FEG-SEM micrographs showing (a) uniform deposition of Ag/ZnO nanorods on the glass substrate. Image in the inset reveals a high deposition of silver nanoparticles. (b) Bunch of ZnO nanorods with immobilized AgNPs. (c) Elemental mapping done for the selected region revealed the presence of zinc (Zn, blue), oxygen (O, white), silver (Ag, green) and silicon (Si, red). Surface composition of the substrate was based on EDX analysis, with characteristic peak of silver at ~ 2.9 kV in addition to other elements
170x133mm (600 x 600 DPI)



FEG-TEM micrograph of (a) a single ZnO nanorod with uniform immobilization of silver nanoparticles. (b) Side view of Ag/ZnO nanorods and immobilized AgNP at the tip of ZnO (inset). HRTEM image (c) showing a distinct interface between Ag and ZnO. High resolution micrographs of ZnO (d) and silver nanoparticles (e) with characteristic d-spacing. Corresponding diffraction patterns of ZnO (above panel) and silver (below panel) are also presented
146x98mm (300 x 300 DPI)

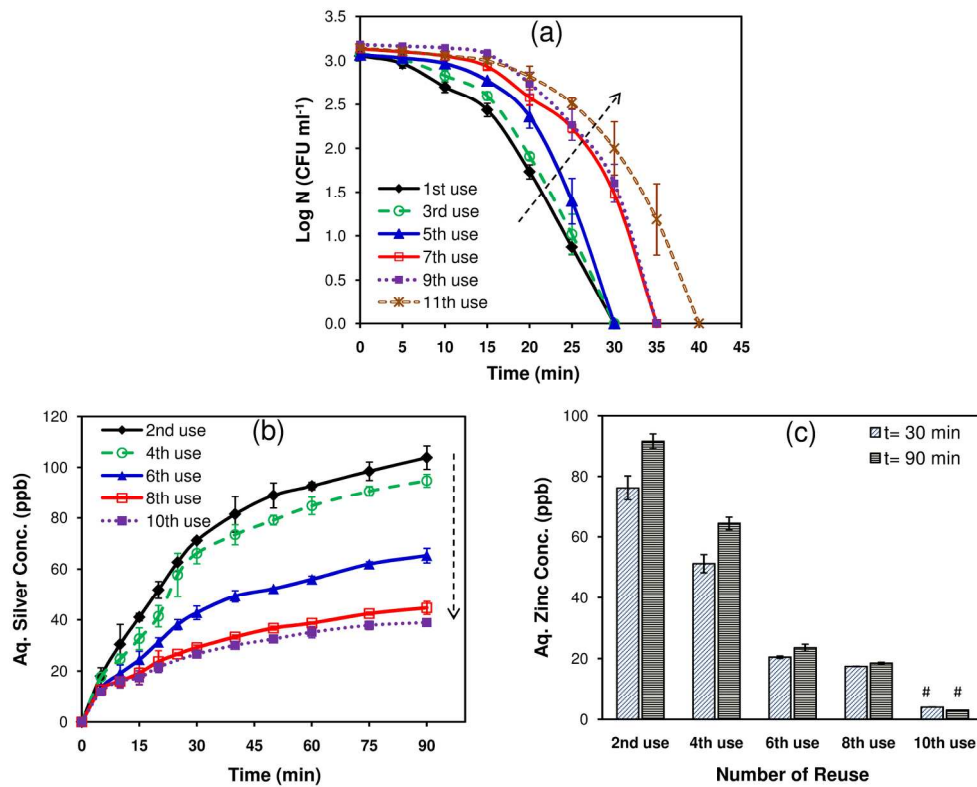


(a) Comparative disinfection potential of pure ZnO nanorods, AgNP immobilized ZnO nanorods (Ag/ZnO HNRs) and colloidal AgNPs (12 ± 2 nm, 6.0×10^{-2} mg in mass). All disinfection studies were performed using *E. coli* MTCC 443 strain (initial cell concentration, $\sim 10^3$ CFU ml⁻¹) in a 100 ml batch reactor. (b) Zone of inhibition (ZoI) tests done at relatively higher bacterial counts (10^5 - 10^6 CFU ml⁻¹) showing the bacteriostatic effect of Ag/ZnO HNRs while no ZoI was observed in case with pure ZnO nanorods
159x168mm (300 x 300 DPI)



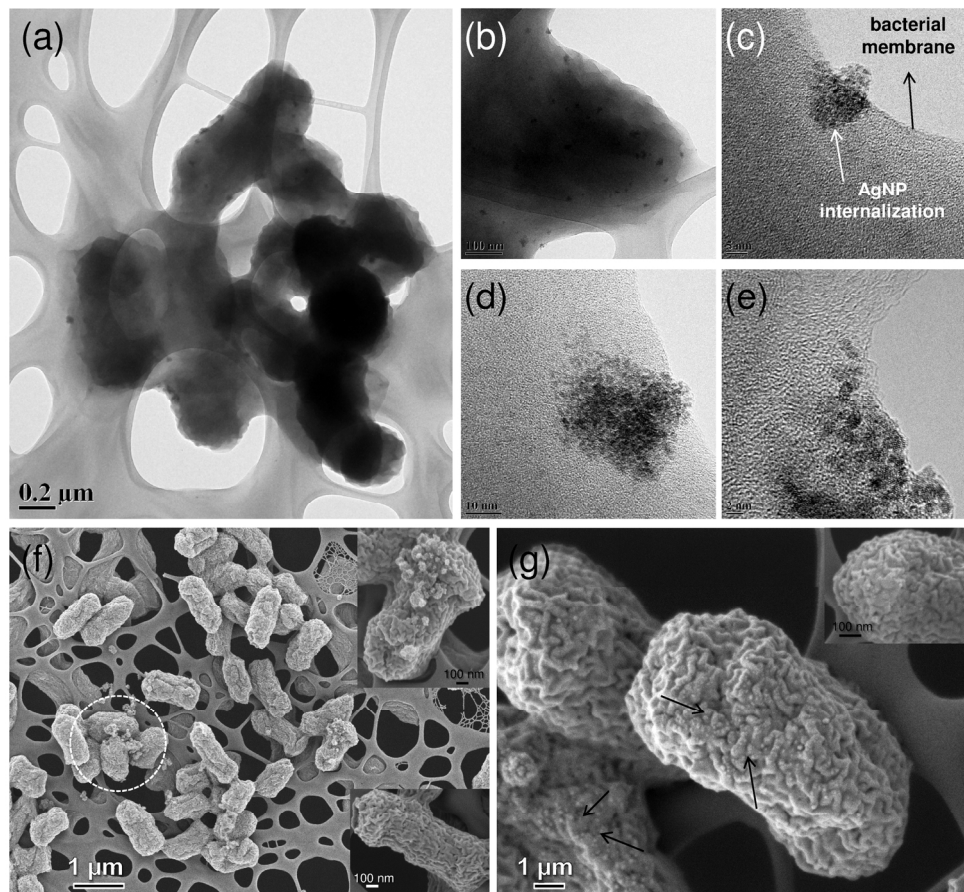
Strain-specific antibacterial activity of Ag/ZnO hybrid nanorods ($2 \times 2.3 \text{ cm}^2$) against (a) Gram-negative, *E. coli* MTCC 443 and (b) Gram-positive, *B. subtilis* MTCC 441 strain. For each strain, disinfection kinetics was tested at an initial concentration of 10^3 CFU ml^{-1} (triangle) and 10^5 CFU ml^{-1} (square) in both, deionized water (continuous line) and phosphate buffer medium (dashed line)

98x40mm (300 x 300 DPI)

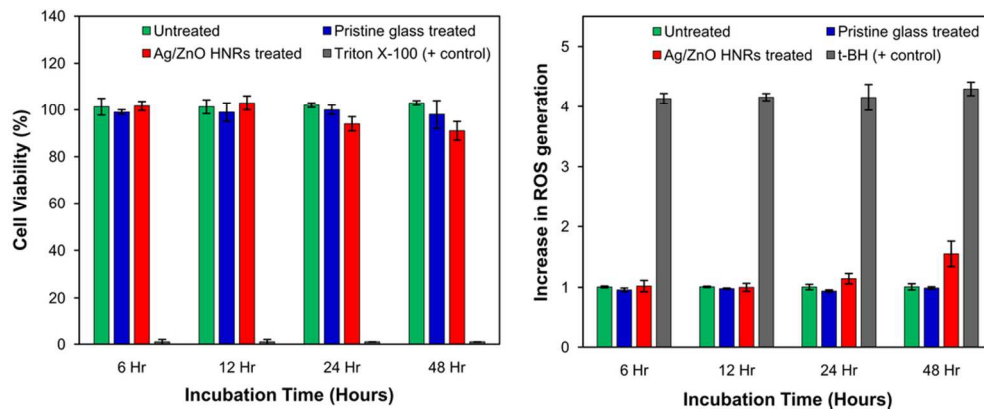


(a) Disinfection performance of a single Ag/ZnO HNR substrate (2 x 2.3 cm²) after 11 times repeated usage against *E. coli* MTCC 443 (10³ CFU ml⁻¹). (b) Corresponding silver release profile (b) after every usage was evaluated. (c) Zinc release after each use over 30 min and 90 minute duration. (# below the detection limit)

181x144mm (300 x 300 DPI)



FEG-TEM (a-e) and FEG-SEM (f-g) analyses of *E. coli* cells (bacterial count, 10^6 - 10^7 CFU ml⁻¹) treated with Ag/ZnO HNR loaded substrate. (a) Lower and (b) higher magnification showing the presence of AgNPs, both near the cell membrane and in the interiors of bacterial cells. (c) An early and (d) late stage of internalization of AgNP aggregates (white arrow) near the cell membrane (black arrow). (e) Crystalline structure reveals the presence of silver in its Ag⁰ state, *i.e.*, AgNPs. SEM images of (f) damaged *E. coli* cells with ruptured morphology (inset, above) and formation of pits and holes on the bacterial surface (inset, below). (g) Silver nanoparticles were homogeneously present all over the surface of bacterial cells
157x146mm (300 x 300 DPI)



Cytotoxicity analysis of Ag/ZnO hybrid nanorods on human hepatocarcinoma (HepG2) cells as determined by (a) MTT assay and (b) intracellular ROS generation. Cells were treated with Ag/ZnO HNRs deposited on glass substrate ($1 \times 1 \text{ cm}^2$) and pristine glass substrate ($1 \times 1 \text{ cm}^2$) for various time periods and (a) percentage of cells viability (b) intracellular ROS level was evaluated after each treatment. Triton X-100 and tertiary butyl hydroperoxide (t-BH) were taken as positive control for MTT and ROS determination experiments, respectively. Experiments were performed in triplicate; data shown are expressed as mean \pm standard error 93x38mm (300 x 300 DPI)